

# Effective source approach to self-force calculations

Ian Vega<sup>1</sup>, Barry Wardell<sup>2</sup>, Peter Diener<sup>3,4</sup>

<sup>1</sup> Department of Physics, University of Guelph, Guelph, Ontario, N1G 2W1, Canada

<sup>2</sup> Max-Planck-Institut für Gravitationsphysik, Albert-Einstein-Institut, 14476 Potsdam, Germany

<sup>3</sup> Center for Computation and Technology, Louisiana State University, Baton Rouge, LA 70803, U.S.A.

<sup>4</sup> Department of Physics and Astronomy, Louisiana State University, Baton Rouge, LA 70803, U.S.A.

E-mail: [ianvega@uoguelph.ca](mailto:ianvega@uoguelph.ca), [barry.wardell@aei.mpg.de](mailto:barry.wardell@aei.mpg.de),  
[diener@cct.lsu.edu](mailto:diener@cct.lsu.edu)

**Abstract.** Numerical evaluation of the self-force on a point particle is made difficult by the use of delta functions as sources. Recent methods for self-force calculations avoid delta functions altogether, using instead a finite and extended “effective source” for a point particle. We provide a review of the general principles underlying this strategy, using the specific example of a scalar point charge moving in a black hole spacetime. We also report on two new developments: (i) the construction and evaluation of an effective source for a scalar charge moving along a generic orbit of an arbitrary spacetime, and (ii) the successful implementation of hyperboloidal slicing that significantly improves on previous treatments of boundary conditions used for effective-source-based self-force calculations. Finally, we identify some of the key issues related to the effective source approach that will need to be addressed by future work.

## 1. Introduction

One of the most important sources of low-frequency gravitational waves for the LISA satellite are the so-called extreme-mass-ratio binary inspirals (EMRIs). These systems consist of a massive black hole (such as those believed to reside in the centers of most galaxies) and a solar mass compact object orbiting around it. A typical mass ratio ( $\mu/M$ ) for these systems would be around  $10^{-6}$ . The compact object gradually spirals into the massive black hole, making  $O(M/\mu)$  full revolutions before making a final plunge that takes place in just one dynamical time scale.

The science potential underlying the detection and measurement of EMRIs by LISA is tremendous [1]. But in order to gain the most science from LISA, exquisitely accurate models of these astrophysical events must be readily available. The benchmark goal is to accurately predict the phase of EMRI gravitational waveforms throughout the entire inspiral. This remains an outstanding challenge.

The small mass ratio reflects the huge disparity of physical scales characterizing EMRIs, and this disparity in turn is the main reason why EMRIs are such a challenge to model numerically. Modeling these systems requires long evolutions of over  $M/\mu$  cycles, and very high spatial resolutions in order to account for the dynamics of the much smaller compact object. These conditions prove to be prohibitive given the current reach of numerical relativity.

On the other hand, the small mass ratio is a clear invitation for the use of the venerable tools of black hole perturbation theory. From this perspective, the compact object can be reliably replaced by a point mass. The emphasis then is on how the presence of the point mass perturbs the spacetime of the larger massive black hole, which ultimately manifests in the wave zone as gravitational waves. By working with a point mass, an assertion is made that the internal degrees-of-freedom of the small compact object are negligible and that its bulk motion is the only relevant property for the purpose of waveform calculations. All this is warranted by the extreme mass ratio involved.

Gravitational wave emission by point masses moving around black hole spacetimes has been studied for a long time, starting with early calculations by Davis *et.al.* [2] and Detweiler [3], which all rely on the seminal works of Regge and Wheeler [4], Zerilli [5], and Teukolsky [6]. In all of the early waveform calculations, the motion of the particle was assumed to be geodesic, so that while the perturbation on the metric is calculated, the back reaction of this perturbation on the motion of the particle was ignored. For LISA-specific data analysis requirements, such back reaction effects must be taken into account. Specifically, in order to accurately track the phase of the gravitational waveform, it is essential to include corrections to geodesic motion arising from the influence of the *self-force*.

The genesis of contemporary self-force analysis can be traced back to derivations by Mino, Sasaki and Tanaka [7], and Quinn and Wald [8], who independently derived a formal expression for the self-force that is now called the MiSaTaQuWa equation.

(An analogous expression for the scalar charge was derived by Quinn [9].) Since these early derivations, much of the work on the self-force has focused on developing practical tools for its evaluation. (It is notable, however, that more rigorous derivations of the gravitational self-force have recently been provided by Gralla and Wald [10] and Pound [11].)

The challenge in evaluating the self-force can be traced to the fact that it is formally given by an integral of the retarded Green function over the entire past history of the particle. Except for rather trivial trajectories in simple spacetimes (e.g. a static particle on Schwarzschild), this integral cannot be done analytically. Moreover, even as one resorts to numerical evaluation, caution must be taken in handling the distributional nature of the source and the singular fields naturally associated with point particles. All this notwithstanding, after more than a decade of effort by various workers, a standard practical method of self-force evaluation has emerged. First proposed by Barack and Ori [12], it has come to be known as the *mode sum method*. This technique has since been implemented to compute self-forces on particles for a variety of cases [13, 14, 15, 16, 17, 18, 19, 20, 21, 22, 23].

#### *Barack-Ori mode sum method*

The Barack-Ori mode sum method is a practical regularization scheme that removes unnecessary pieces from the retarded field of a particle, ultimately resulting in the self-force. It is so named because it builds upon a decomposition of the retarded field into spherical-harmonic modes.

For concreteness, we shall consider the case of a minimally-coupled scalar charge moving in a black hole spacetime. This is a simpler toy problem that, from the standpoint of self-force evaluation, nevertheless shares much of the key technical features of the point mass case. The relevant field equation, in this case, is given by

$$\square\Phi^{\text{ret}} = q\delta(x, x_0(\tau)) \quad (1)$$

where  $\square$  is the curved spacetime d'Alembertian, and  $\delta(x, x_0(\tau))$  is the four-dimensional Dirac delta function representing the scalar particle of charge  $q$ , whose worldline is given by  $x_0(\tau)$ . The resulting retarded field,  $\Phi^{\text{ret}}$ , and its gradient,  $\nabla_\alpha\Phi^{\text{ret}}$ , are singular at the location of the particle. However, the mode sum approach takes advantage of the fact that the spherical harmonic  $l$ -modes of the gradient of the retarded field,  $(\nabla_\alpha\Phi^{\text{ret}})_l$ , defined through

$$\nabla_\alpha\Phi^{\text{ret}} = \sum_l (\nabla_\alpha\Phi^{\text{ret}})_l = \sum_l \left( \sum_{m=-l}^l (\nabla_\alpha\Phi^{\text{ret}})_{lm} \right), \quad (2)$$

all turn out to be finite at the particle's location. Being finite, each of the modes can be computed numerically. Certain pieces are then subtracted from each of these modes in such a way that the remainders sum up to the correct finite self-force. These pieces are derived from a careful local analysis of the singular structure of the retarded field at the particle's location, and are codified in so-called *regularization parameters*,  $\{A_\alpha, B_\alpha, C_\alpha, \dots\}$ , which depend only on the background spacetime and on the orbital

parameters describing the motion of the particle [24, 25, 26, 17, 19]. As such, the self-force is computed as

$$F_\alpha = \sum_l \left[ (\nabla_\alpha \Phi^{\text{ret}})_l - (A_\alpha)(l + 1/2) - B_\alpha - \frac{C_\alpha}{l + 1/2} - \dots \right]. \quad (3)$$

This mode sum will converge with the use of only the first three regularization parameters  $\{A_\alpha, B_\alpha, C_\alpha\}$ .

### Detweiler-Whiting decomposition

Understanding of the Barack-Ori mode sum method was enriched by Detweiler and Whiting's (DW) discovery [27] that the self-force on a particle can be entirely attributed to a (smooth) solution of the homogeneous field equation:

$$\square \Phi^{\text{R}} = 0, \quad (4)$$

$$F_\alpha = \nabla_\alpha \Phi^{\text{R}}, \quad (5)$$

where  $\Phi^{\text{R}}$  is known as the *regular field*. This is akin to Dirac's [28] classic result in the flat spacetime case showing that radiation reaction is due solely to the “half-retarded minus half-advanced” field, which is a smooth homogeneous solution of the wave equation.

A key point in the DW analysis was the correct identification of the *singular field*,  $\Phi^{\text{S}}$ , which is the part of the retarded field that has no contribution to the self-force. The singular field is a solution of the same inhomogeneous field equation as  $\Phi^{\text{ret}}$  in the normal neighborhood of the particle's location:

$$\square \Phi^{\text{S}} = q\delta(x, x_0(\tau)), \quad x \in \mathcal{N}_{x_0}, \quad (6)$$

where we denote the normal neighborhood by  $\mathcal{N}_{x_0}$ . As such, the singular field shares the same singularity structure as the retarded field, and yet it differs from the retarded field in that it does not depend on the details of the particle's distant past history.

The regular field is then essentially the difference between retarded and singular fields:

$$\Phi^{\text{R}} := \Phi^{\text{ret}} - \Phi^{\text{S}}. \quad (7)$$

Therefore, from (5), the self-force is

$$F_\alpha = (\nabla_\alpha \Phi^{\text{ret}} - \nabla_\alpha \Phi^{\text{S}})|_{x=x_0}, \quad (8)$$

from which the regularization parameters of (3) turn out, in effect, to be just the  $l$ -modes of  $\nabla_\alpha \Phi^{\text{S}}$  evaluated at  $x_0$ .

### An elementary self-force calculation

It is pedagogically useful to note that a self-force calculation is already encountered in any undergraduate course in electromagnetism. We recall the problem of a point charge  $q$  in the vicinity of an infinite grounded conducting plane. A standard problem is to compute the force that needs to be exerted on the charge in order to keep it at a fixed distance away from the plane. For concreteness, assume that  $q$  is located at  $\mathbf{x}_0 = (0, 0, a)$ , in Cartesian coordinates, and that the conducting plane is at  $z = 0$ .

This problem may of course be solved with the method of images. In order to maintain a zero electrostatic potential along the conducting plane, one imagines an image charge,  $-q$ , located at  $-\mathbf{x}_0$ . The full electric field,  $\mathbf{E}^{\text{full}}$ , around  $q$  will be the superposition of the electric fields due to the real and image charges, say  $\mathbf{E}^{(q)}$  and  $\mathbf{E}^{(-q)}$ , respectively. The electric field,  $\mathbf{E}^{\text{full}}$ , is what is felt by an observer in the vicinity of the  $q$ , but it is singular at the location of  $q$ .

Now, to compute the force on the real charge, one just subtracts its Coulomb field from the full electric field, giving

$$\mathbf{F} = q(\mathbf{E}^{\text{full}} - \mathbf{E}^{(q)}) = q\mathbf{E}^{(-q)} = \frac{q^2}{4a^2}\hat{\mathbf{z}} \quad (\text{in gaussian units}), \quad (9)$$

which is finite at the location of  $q$ . The rationale behind this subtraction is that  $\mathbf{E}^{(q)}$  is isotropic around the charge  $q$ , and therefore cannot exert a net force on it.

The steps in this elementary calculation are directly analogous to more complicated self-force calculations for the case of particles moving in a curved spacetime. It consists of (a) computing the full field,  $\mathbf{E}^{\text{full}}$  (which is the direct analogue of  $\nabla_\alpha\Phi^{\text{ret}}$ ), (b) identifying a singular part of the full field that exerts no force on the charge,  $\mathbf{E}^{(q)}$  (*cf.*  $\nabla_\alpha\Phi^{\text{S}}$ ), and (c) subtracting these two fields to give a smooth remainder at the location of the charge. What remains after this subtraction is then solely responsible for the self-force. For this particular problem, it is  $\mathbf{E}^{(-q)}$  that takes the place of the gradient of the Detweiler-Whiting regular field. It is a solution to the homogeneous field equation in the vicinity of the real charge (and therefore smooth there). It is the force due to this field that must be balanced by some external force in order to keep the charge in a fixed location.

## 2. Self-force from an effective source

The perspective arising from the work of Detweiler and Whiting is that a self-force calculation amounts to computing the smooth regular field,  $\Phi^{\text{R}}$ , and evaluating its gradient at the particle's location. This idea motivates new strategies for self-force calculation. One specific strategy enables the use (2+1) and (3+1) grids. The ideas of this section were first independently presented by Barack and Gollub [29, 30] and Vega and Detweiler [31]. Development of (2+1) [32] and (3+1) [33] codes for self-force calculations has since continued to progress.

As pointed out in the previous section, the traditional focus in a self-force calculation was on first solving (1) for the retarded field. This is difficult because delta functions are not easily represented on a numerical grid. Moreover, it is not clear how to represent the retarded field on a (3+1) grid, given its singular nature at the particle location. Both issues can be circumvented by adopting the DW strategy of splitting the retarded field into its (smooth) regular and (non-smooth) singular parts. The idea is simple. Writing (1) in terms of  $\Phi^{\text{R}}$  and  $\Phi^{\text{S}}$ , we have

$$\square(\Phi^{\text{R}} + \Phi^{\text{S}}) = q\delta(x, x_0) \quad x \in \mathcal{N}_{x_0} \quad (10)$$

$$\rightarrow \square\Phi^{\text{R}} = 0 \quad x \in \mathcal{N}_{x_0}. \quad (11)$$

Thus, given an analytic expression for  $\Phi^S$ , the original field equation for  $\Phi^{\text{ret}}$  can be converted into a homogeneous equation for  $\Phi^R$ . Now this may look a bit unsettling because we seem to have made the source disappear entirely; the explicit dependence of the fields on  $q$  is apparently lost. But one must not overlook the fact that (11) is actually valid only in the normal neighborhood of the particle. The singular field is well-defined only in the normal neighborhood, and therefore (11) is likewise restricted to only this region.

To compute  $\Phi^R$ , one needs to supplement (11) with boundary conditions on the boundary<sup>‡</sup> of the normal neighborhood,  $\partial\mathcal{N}_{x_0}$ . These conditions will depend on the values of the singular and retarded fields on  $\partial\mathcal{N}_{x_0}$  (and thus on  $q$ ). The retarded field outside the normal neighborhood will arise from solving the same homogeneous field equation with outgoing wave boundary conditions at infinity and another condition on its inner boundary  $\partial\mathcal{N}_{x_0}$  enforcing consistency between  $\Phi^R$ ,  $\Phi^S$ , and  $\Phi^{\text{ret}}$ . Altogether then, the splitting of the retarded field turns the original field equation into

$$\square\Phi^R = 0, \quad x \in \mathcal{N}_{x_0} \tag{12}$$

$$\square\Phi^{\text{ret}} = 0, \quad x \notin \mathcal{N}_{x_0} \tag{13}$$

together with the matching condition  $\Phi^{\text{ret}} = \Phi^R + \Phi^S$  at the boundary  $\partial\mathcal{N}_{x_0}$ , and outgoing wave boundary conditions at infinity. Thus, the DW splitting of the retarded field has turned (1) into homogeneous field equations for  $\Phi^R$  and  $\Phi^{\text{ret}}$  in two separate computational domains.

Without delta functions as sources, this set-up can now be tackled more readily on a numerical grid. Moreover, since one would be solving for  $\Phi^R$ , which is smooth at the particle, no regularization is necessary to evaluate the self-force; one would simply have to evaluate  $\nabla_\alpha\Phi^R$  at the location of the particle. And finally, scalar radiation waveforms are also just as easily computed by evaluating the retarded field in the wave zone.

From a practical standpoint, the use of  $\partial\mathcal{N}_{x_0}$  as the boundary for the two distinct computational domains is bound to be inconvenient. Fortunately, this is not actually necessary. One is in fact permitted to choose any boundary so long as a singular field can be explicitly computed on it and an appropriate matching condition between  $\Phi^{\text{ret}}$  and  $\Phi^R$  can be enforced. If one chooses a boundary outside  $\mathcal{N}_{x_0}$ , then strictly speaking the DW singular field will no longer be defined there, and an extension of the singular field, call it  $\bar{\Phi}^S$ , will be needed. This extended singular field must mimic the DW singular field close to the particle, but can be different anywhere else. Any extension will suffice provided that  $\bar{\Phi}^S$  and  $\square\bar{\Phi}^S$  are finite and calculable at the boundary, though ideally, one would want to choose a smooth extension so as not to introduce any unnecessary non-smoothness in the effective source. These considerations emphasize the point that the essential part of the DW singular field is its behaviour close to the particle. (Barack and Golbourn [29] call these extensions of  $\Phi^S$  *punctures*. Their original notion of ‘‘puncture’’

<sup>‡</sup> Strictly speaking, the singular field is only defined inside the normal neighborhood and not its boundary. The boundary condition must then be applied just inside the normal neighborhood boundary. We therefore define  $\partial\mathcal{N}_{x_0}$  to be the boundary just inside the edge of the normal neighborhood.

included the requirement that it have a straightforward  $m$ -mode expansion. But in [32] they have since adopted the DW singular field as a starting point.)

With the freedom in choosing  $\bar{\Phi}^S$ , it is also possible to completely avoid having to use two separate computational domains [31, 33]. The trick is to simply choose  $\bar{\Phi}^S$  to be a modulated version of the original singular field, such that  $\bar{\Phi}^S$  is forced to vanish outside an arbitrarily chosen neighborhood of the particle. This is achieved with a smooth window function,  $W$ , that is compactly supported within this neighborhood. As an example, consider the choice  $\bar{\Phi}^S := W\Phi^S$ , such that  $W$  smoothly transitions to zero as it approaches  $\partial\mathcal{N}_{x_0}$  and is zero everywhere outside  $\mathcal{N}_{x_0}$ . The redefined regular field would then be  $\bar{\Phi}^R := \Phi^{\text{ret}} - W\Phi^S$ . In this case, the window function already forces  $\bar{\Phi}^R$  to equal  $\Phi^{\text{ret}}$  at  $\partial\mathcal{N}_{x_0}$  and outside  $\mathcal{N}_{x_0}$ , so that no matching would have to be imposed at  $\partial\mathcal{N}_{x_0}$ . The resulting field equation is then

$$\square\bar{\Phi}^R = q\delta(x, x_0(\tau)) - \square(W\Phi^S). \quad (14)$$

Notice now that no distinction is drawn between the original two computational domains, and the only boundary conditions that need to be imposed are those at infinity. Outside the chosen neighborhood, the source on the right hand side vanishes, and so one is left with the (homogeneous) field equation for the retarded field. The new field,  $\bar{\Phi}^R$ , thus smoothly transitions into  $\Phi^{\text{ret}}$ , and a single computational domain for  $\bar{\Phi}^R$  would suffice.

The window function must satisfy certain conditions for the new regular field to retain the property that its gradient at the particle also equals the correct self-force, just as the original DW regular field. The necessary conditions which must be imposed on  $W$  are:

- (i)  $W = 1 + f$ , such that  $f \rightarrow O(\epsilon^n)$  and  $\nabla_\alpha f \rightarrow O(\epsilon^{n-1})$  as  $\epsilon \rightarrow 0$ ;
- (ii)  $W$  is smooth;
- (iii)  $W = 0$ ,  $x \notin \mathcal{N}_{x_0}$ ,

where  $\epsilon$  is some measure of distance away from the worldline, and  $n$  is an integer that must be  $\geq 3$ . The lower bound in  $n$  comes from the requirement that each of the last two terms on the right hand side of

$$\nabla_\alpha\bar{\Phi}^R = \nabla_\alpha(\Phi^{\text{ret}} - \Phi^S) - (\nabla_\alpha f)\Phi^S - f(\nabla_\alpha\Phi^S) \quad (15)$$

vanish as  $\epsilon \rightarrow 0$ , i.e. as the particle is approached. Close to the particle both the singular and retarded fields behave like Coulomb fields in that they diverge as  $\Phi^S \sim O(\epsilon^{-1})$  and  $\nabla_\alpha\Phi^S \sim O(\epsilon^{-2})$ . Condition (i) ensures that  $\bar{\Phi}^R$  does not differ from  $\Phi^R$  in any essential way as one approaches the particle, so that the gradient of  $\bar{\Phi}^R$  at the location of the charge still gives the correct self-force.

The field equation to be solved for  $\bar{\Phi}^R$  is then simply

$$\square\bar{\Phi}^R = \mathcal{S}_{\text{eff}}(x, x_0, u_0), \quad (16)$$

where the *effective source* is defined to be

$$\mathcal{S}_{\text{eff}} := q\delta(x, x_0) - \square(W\Phi^S). \quad (17)$$



This effective source is *smooth*, and will depend on the position,  $x_0^\alpha$ , and four-velocity,  $u_0^\alpha$ , of the particle. The delta function of the first term is cancelled by another delta function coming from the second term:

$$\begin{aligned}\mathcal{S}_{\text{eff}} &= q\delta(x, x_0) - \nabla_\alpha W \nabla^\alpha \Phi^S - \Phi^S \square W - W \square \Phi^S \\ &= (q\delta(x, x_0) - W \square \Phi^S) - \nabla_\alpha W \nabla^\alpha \Phi^S - \Phi^S \square W \\ &= -f\delta(x, x_0) - \nabla_\alpha W \nabla^\alpha \Phi^S - \Phi^S \square W \\ \mathcal{S}_{\text{eff}} &= -\nabla_\alpha W \nabla^\alpha \Phi^S - \Phi^S \square W.\end{aligned}$$

The third line follows from the fact that the singular field,  $\Phi^S$ , is a local solution to the inhomogeneous field equation. The delta function no longer appears in the last line because  $f$  is chosen to vanish on the worldline.

Solving for  $\bar{\Phi}^R$  in (16) with whatever numerical method one prefers, the self-force is then just

$$F_\alpha = (\nabla_\alpha \bar{\Phi}^R)|_{x=x_0}. \quad (18)$$

### 3. Generic effective source for a scalar point charge

In the previous section, we expounded on the idea of evaluating the self-force by solving the field equations with a *smooth* effective source,  $\mathcal{S}_{\text{eff}}$ , as defined by (17). To emphasize that this source does not contain a delta function, we may rewrite this as

$$\mathcal{S}_{\text{eff}} = \begin{cases} 0, & x = x_0 \\ -\square(W\Phi^S), & x \neq x_0. \end{cases} \quad (19)$$

If a window function is not used,  $\mathcal{S}_{\text{eff}}$  simplifies considerably, since it completely vanishes inside the normal neighborhood. As already indicated, a boundary around the particle would then have to be chosen where the matching condition between  $\Phi^{\text{ret}}$  and  $\Phi^R$  is to be imposed. These statements assume, however, that an *exact* expression for  $\Phi^S$  is available, which unfortunately is true only for the simplest of cases (e.g. a static particle in static black hole spacetimes). Generally, only an approximation to  $\Phi^S$  is attainable, and the best one can do is to write

$$\Phi^S = \tilde{\Phi}^S + O(\epsilon^n), \quad (20)$$

where  $\tilde{\Phi}^S$  approximates the exact singular field up to terms that scale as  $\epsilon^n$ , as  $\epsilon \rightarrow 0$ . As a result, the effective source will generally not vanish in the vicinity of the particle.

Consequently, the effective source method rests on the ability to write down an expression for (a non-zero)  $\mathcal{S}_{\text{eff}}$  in terms of the coordinates in which one wishes to solve the field equation. This shall be the focus of the present section. In this section, we shall rely on the methods of bi-tensor theory, as covered by Poisson [34].

Writing down the effective source essentially amounts to taking derivatives of the Detweiler-Whiting singular field (and the window function, if one chooses to use one). The DW singular field is defined through the singular Green function

$$G^S(x, x') = \frac{1}{2}U(x, x')\delta(\sigma(x, x')) + \frac{1}{2}V(x, x')\theta(\sigma(x, x')), \quad (21)$$



where  $U(x, x')$  and  $V(x, x')$  are bi-scalars that are regular for  $x \rightarrow x'$ . This form of the Green function is valid so long as  $x$  and  $x'$  are connected by a unique geodesic; that is, in the normal neighborhoods of  $x$  and  $x'$ .

With this, the singular field is

$$\Phi^S = q \int_{\gamma} G^S(x, z(\tau)) d\tau, \quad (22)$$

where the integration is taken over the worldline of the particle,  $\gamma$ . The singular Green function has support only when  $\sigma(x, x') \geq 0$ ; that is, when  $x$  and  $x'$  are either null- or spacelike-related. This restricts the domain of integration to a mere portion of the worldline. With a change of variable from  $\tau$  to  $\sigma$ , one can re-express this as

$$\Phi^S = \frac{q}{2\sigma_{\alpha'} u^{\alpha'}} U(x, x') - \frac{q}{2\sigma_{\alpha''} u^{\alpha''}} U(x, x'') - \frac{q}{2} \int_u^v V(x, z(\tau)) d\tau, \quad (23)$$

where  $\sigma_{\alpha'} := \sigma_{\alpha'}(x, x')|_{x'=z(u)}$ ,  $\sigma_{\alpha''} := \sigma_{\alpha''}(x, x'')|_{x''=z(v)}$ , and  $u$  and  $v$  are the retarded and advanced times. Respectively, they are defined to be the proper times (along  $\gamma$ ) at which a past-directed and future-directed null geodesics emanating from  $x$  intersect the worldline. The retarded and advanced times depend implicitly on  $x$  uniquely through the relations  $\sigma(x, z(u)) = 0$  and  $\sigma(x, z(v)) = 0$ .

### 3.1. Haas-Poisson expression for the singular field

The expression for the singular field given in (23) is very general. It is valid for any worldline in any spacetime provided the field point  $x$  is sufficiently close to the worldline that the singular Green function can be defined (i.e. within the normal neighborhood). In practice, it is only in very simple spacetimes that  $U(x, x')$ ,  $U(x, x'')$ ,  $\sigma$  and  $V(x, x')$  may be computed exactly. In many curved spacetimes of interest (including Schwarzschild and Kerr) this is not the case and one must find an approximation to (23).

In the present work, we choose a covariant series expansion of (23), taken to second order in the geodesic distance from the field point to the world line, as an approximation to  $\Phi^S$ . In doing so, we use the methods described in Refs. [34] and [19] to consolidate the dependence of  $\Phi^S$  on the advanced and retarded points  $x'$  and  $x''$  into a single arbitrary point  $\bar{x}$  on the worldline. This has the additional advantage of making the dependence of  $x'(x)$  and  $x''(x)$  on  $x$  explicit, so that  $\bar{x}$  is truly an arbitrary point on the worldline (sufficiently close to  $x'$  and  $x''$ ) with no implicit dependence on  $x$ . We additionally make use of the techniques of Ref. [35] to compute covariant expansions of all required bi-tensors.

Given the primary motivation of studying black hole spacetimes such as Schwarzschild and Kerr, we make the assumption that the spacetime is vacuum (i.e.  $R_{ab} = 0$ ). In doing so, we find that near to the world-line

$$\begin{aligned} U(x, x') &\approx U(x, x'') = 1 + \mathcal{O}(\epsilon^4) \\ V(x, z(\tau)) &= \mathcal{O}(\epsilon^4). \end{aligned} \quad (24)$$

For an  $\mathcal{O}(\epsilon)$  effective source, we must keep terms in  $U(x, x')$  and  $U(x, x'')$  up to  $\mathcal{O}(\epsilon^3)$  and in  $V(x, z(\tau))$  up to  $\mathcal{O}(\epsilon)$ . We therefore find that our approximation to  $\Phi_S$  takes the simpler form

$$\Phi^S = \frac{q}{2\sigma_{\alpha'}u^{\alpha'}} - \frac{q}{2\sigma_{\alpha''}u^{\alpha''}} + \mathcal{O}(\epsilon^3). \quad (25)$$

Next, we follow Haas and Poisson in expanding the quantities  $r_- = \sigma_{\alpha'}u^{\alpha'}$  and  $r_+ = -\sigma_{\alpha''}u^{\alpha''}$  about the arbitrary point  $\bar{x}$ :

$$r_{\pm} \approx s - \frac{\bar{r}^2 - s^2}{6s} R_{u\sigma u\sigma} - \frac{\bar{r} - s}{24s} [(\bar{r} \pm s)(\bar{r} \mp 2s) R_{u\sigma u\sigma|u} - (\bar{r} \pm s) R_{u\sigma u\sigma|\sigma}], \quad (26)$$

where  $s^2 := (g^{\bar{\alpha}\bar{\beta}} + u^{\bar{\alpha}}u^{\bar{\beta}})\sigma_{\bar{\alpha}}\sigma_{\bar{\beta}}$  (i.e. the projection of  $\sigma_{\bar{a}}$  orthogonal to the worldline), and  $\bar{r} = \sigma_{\bar{\alpha}}u^{\bar{\alpha}}$  (the projection along the worldline) and we adopt the notation of Haas and Poisson [19] in defining  $R_{u\sigma u\sigma|\sigma} \equiv R_{\bar{\alpha}\bar{\beta}\bar{\gamma}\bar{\delta};\bar{\epsilon}}u^{\bar{\alpha}}\sigma^{\bar{\beta}}u^{\bar{\gamma}}\sigma^{\bar{\delta}}\sigma^{\bar{\epsilon}}$ . Substituting these expansions into (25), we get

$$\Phi^S = q \left\{ \frac{1}{s} + \left[ \frac{\bar{r}^2 - s^2}{6s^3} R_{u\sigma u\sigma} \right] + \left[ \frac{1}{24s^3} (\bar{r}^2 - 3s^2) \bar{r} R_{u\sigma u\sigma|u} - (\bar{r}^2 - s^2) R_{u\sigma u\sigma|\sigma} \right] + \mathcal{O}(\epsilon^3) \right\}. \quad (27)$$

Letting  $\epsilon$  be a measure of the geodesic distance from  $x$  to the world-line (i.e.  $\bar{x}$ ), the first term here is  $\mathcal{O}(\epsilon^{-1})$ , the second group of terms is  $\mathcal{O}(\epsilon^1)$  and the third group of terms is  $\mathcal{O}(\epsilon^2)$ . The error in this approximation to  $\Phi_S$  is then  $\mathcal{O}(\epsilon^3)$ .

The final step is to convert this covariant expression for the singular field to an expression in terms of the coordinates of the background spacetime. This is easily achieved by using the methods of [19] or [36] to rewrite  $\sigma^{\bar{a}}$  as a coordinate expansion and then substituting the result into (27).

With the coordinate expression for the approximate singular field at hand, what remains to be done in order to get  $\mathcal{S}_{\text{eff}}$  is to apply the d'Alembertian on the singular field. In Fig. 1 we give plots demonstrating the result of this calculation for the case of a particle in a circular equatorial orbit (at  $r = 10M$ ) around a Schwarzschild black hole. The surface plots give the value of the singular field and effective source along the equatorial plane. The shown approximation to the singular field differs from the exact singular field at  $\mathcal{O}(\epsilon^3)$  and hence the effective source differs from the exact effective source at  $\mathcal{O}(\epsilon)$ . As there was no window function (equivalently  $W = 1$ ) used in generating these plots, the exact effective source would be 0 and so the approximate effective source is  $\mathcal{S}_{\text{eff}} = 0 + \mathcal{O}(\epsilon)$ . In this plot, the particle is at the point where there appears to be a pinch in the curve.

We emphasize that the resulting effective source is for a scalar charge moving along a *generic* geodesic, and that this is the first time an effective source of this sort has appeared in print.

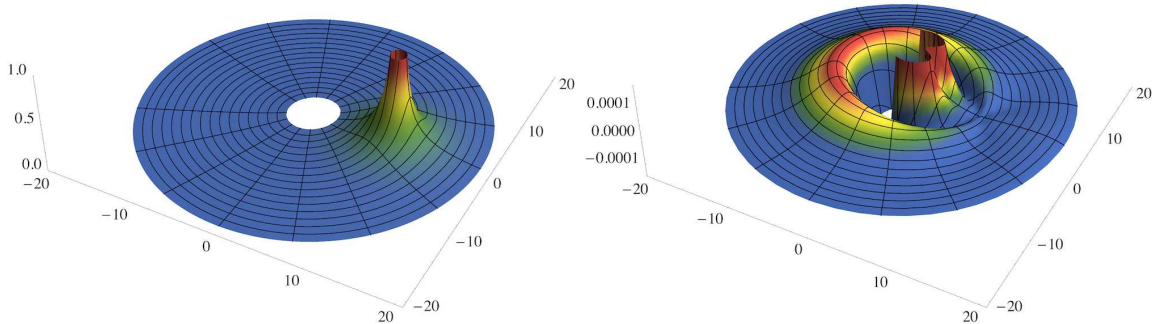


**Figure 1.** (Color online) Approximation to the singular field (left) and corresponding effective source (right) along the equatorial plane for a particle in a circular orbit (at  $r = 10M$ ) around a Schwarzschild black hole.

### 3.2. THZ coordinates

Another route towards the effective source makes use of a convenient set of locally-inertial coordinates first introduced by Thorne and Hartle [37] and Zhang [38]. This would entail directly performing the integration in (22) as expressed in these coordinates. It was through this approach that the first coordinate expression for the scalar singular field was derived (albeit for the restricted case of a circular orbit in Schwarzschild) [17].

The appeal of this coordinate frame, in the self-force context, is due to the fact that they result in the background metric and d'Alembertian taking on particularly convenient forms. As a result, the singular field can be expressed simply as

$$\Phi^S = \frac{q}{\sqrt{X^2 + Y^2 + Z^2}} + O(\epsilon^3) \quad (28)$$

in THZ coordinates  $\{T, X, Y, Z\}$ .

In this form, the complexity of the singular field is hidden in the transformation from the coordinates of the background spacetime,  $\{x\}$ , to the THZ coordinates,  $\{X(x), Y(x), Z(x)\}$ . This transformation was derived explicitly for the case of a circular orbit in the Schwarzschild spacetime [17]. Progress is being made towards deriving this transformation for a generic geodesic in an arbitrary spacetime.

## 4. Issues in evaluating the effective source

### Computational cost

Writing out the coordinate expression for  $\mathcal{S}_{\text{eff}}$  is straightforward enough to do with computer algebra software such as *Mathematica* or *Maple*, but for the order of the approximation that is sought here (i.e.  $\mathcal{S}_{\text{eff}} \sim O(\epsilon)$  as  $\epsilon \rightarrow 0$ ), what results is a massively long expression whose evaluation is potentially very costly in an application requiring the effective source to change *dynamically* in a self-consistent (3+1) simulation. Going from Schwarzschild to the more complicated Kerr geometry further exacerbates this issue.

Given such considerations, computing the d'Alembertian of  $W\Phi^S$  with *numerical* derivatives (instead of evaluating a full analytical expression for the derivatives) becomes worth exploring. Done naively, this strategy is likely going to sacrifice some accuracy, but it is quite possible that this loss of accuracy will be tolerable. We can be optimistic that this is the case given the fact that the d'Alembertian of  $\bar{\Phi}^S$  can be evaluated by numerically computing derivatives of low-order polynomials. One can see this from (27), which can be rewritten as

$$q^{-1}\bar{\Phi}^S = \frac{K}{S^{3/2}}, \quad (29)$$

where

$$K := s^2 + \frac{1}{6}(\bar{r}^2 - s^2)R_{u\sigma u\sigma} + \frac{1}{24}(\bar{r}^2 - 3s^2)\bar{r}R_{u\sigma u\sigma|u} - \frac{1}{24}(\bar{r}^2 - s^2)R_{u\sigma u\sigma|\sigma} \quad (30)$$

$$S := s^2 \quad (31)$$

Both  $K$  and  $S$  when written in, say, Schwarzschild coordinates are just low-order polynomials

$$K = \sum_{\substack{i,j,k,l=2 \\ i+j+k+l=5}} A_{ijkl}(t-T)^i(r-R)^j(\theta-\Theta)^k(\phi-\Phi)^l \quad (32)$$

$$S = \sum_{\substack{i,j,k,l=2 \\ i+j+k+l=5}} B_{ijkl}(t-T)^i(r-R)^j(\theta-\Theta)^k(\phi-\Phi)^l, \quad (33)$$

with  $\{T, R, \Theta, \Phi\}$  denoting the particle's position in these coordinates. Numerical derivatives of these 5th-order polynomials can be computed quite accurately and cheaply.

Exploring how best to compute the effective source with numerical derivatives is left to future work.

### *Catastrophic cancellation near the worldline*

Another serious issue encountered is the potentially severe round-off error incurred when evaluating the effective source close to the particle. This is an issue regardless of one's strategy for computing derivatives. It is easy to understand why this would happen.

The approximate singular field possesses the familiar  $O(\epsilon^{-1})$  Coulombic divergence close to the particle. Consequently, the d'Alembertian acting on  $\bar{\Phi}^S$  results in dominant terms that each scale as  $O(\epsilon^{-3})$ . By construction, however, the effective source ought to scale as  $O(\epsilon)$  as  $\epsilon \rightarrow 0$ . This means that all the  $O(\epsilon^{-3})$ -terms should somehow cancel to give the  $O(\epsilon)$  over-all behaviour of the effective source. This is a typical instance of catastrophic cancellation that can lead to massive round-off errors.

For moderately small  $\epsilon$ , say  $\epsilon = 0.1$ , the subtraction of terms results in a number  $10^{-4}$  times smaller than the magnitude of the terms themselves. This implies a loss of 4 significant digits in the result, which may perhaps still be acceptable (assuming, say, double precision of  $\sim 15$  digits). But closer to the particle, at say  $\epsilon = 10^{-3}$ , one

instead loses 12 significant digits. It is clear then that as one approaches the particle, the evaluation of the effective source becomes increasingly inaccurate. In [33], a very crude “fix” was employed to avoid this concern: whenever an evaluation very close to the particle was needed, a different point slightly farther from the particle was chosen in evaluating the effective source. Remarkably (and rather surprisingly, in retrospect), this cheap fix alone lead to results with errors of  $\lesssim 1\%$ .

The ideal solution to this would be to get the  $O(\epsilon^{-3})$ -terms in the effective source to cancel *analytically*, leaving only a remainder that would then *explicitly* scale as  $O(\epsilon)$ . Unfortunately, the expressions we have worked with turn out to be sufficiently complicated to prohibit this this being done in any obvious manner. (Experiments with analytical expressions in *Mathematica* give us indications that there may be some way of achieving this, but we have not explored this sufficiently to be able to make any concrete statements.)

Another solution to this would be to work towards a covariant expansion of the effective source. Instead of taking (partial) derivatives of the singular field, one can postpone the introduction of coordinates and find an expansion of  $\mathcal{S}_{\text{eff}}$  itself in powers of  $\sigma^{\bar{\alpha}}$ . This provides a clear route for cancelling the divergent terms analytically, but it comes at the expense of introducing errors in the effective source that grow away from the particle. However, if one restricts the use of the covariant expansion to a region very close to the particle ( $\epsilon \ll 1$ ), then these errors are also going to be small and potentially acceptable. With a covariant expression at hand, one possible strategy would be to use it for evaluations close to the particle, and to use the usual expression (i.e., computed with partial derivatives) when one is further away. Work by Ottewill and Wardell [35] has now pushed Hadamard expansions to very high order, allowing for ever more accurate approximations to the singular field. The techniques they developed could be used to derive a high-order covariant effective source that would have a wider region of applicability around the particle.

Finally, if all else fails, a simple polynomial interpolation (see Fig. 2) might be the best fix for this problem. One would identify a small neighborhood around the particle within which round-off reaches unacceptable levels. When the effective source needs to be evaluated at a point inside this region, one would interpolate using effective source values outside the region and the known zero value of the effective source at the location of the particle.

Another immediate goal is to determine an optimal solution to this round-off issue, which is likely going to be a hybrid of the ideas presented here.

## 5. Issues for the effective source approach to self-force calculations

The numerical experiments performed in [33] showed the existence of some serious issues that must be overcome before simulations can be performed for long enough and with high enough accuracy to reliably extract the self-force.

The first problem is the presence of non-physical outer boundaries arising from

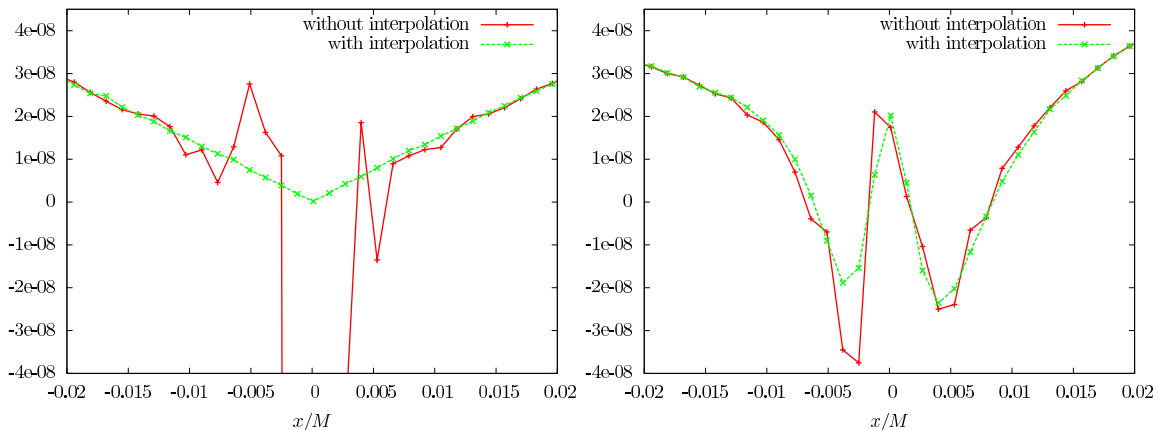


**Figure 2.** (Color online) Interpolation of the effective source. These figures show how a simple interpolation scheme mitigates the round-off errors due to the catastrophic cancellation that occurs in the region very close to the particle. Both figures are plots of  $\mathcal{S}_{\text{eff}}(x, y, z = 0)$ , with  $y/M = 10M$  and  $y/M = 10.005M$  (in Kerr-Schild coordinates), respectively, for a scalar charge moving in a circular orbit of Schwarzschild at  $r = 10M$ , where  $r$  is the Schwarzschild radial coordinate. The scalar charge is located at  $(x = 0, y = 10M, z = 0)$ . The plot on the left clearly shows the  $C^0$  nature of the effective source at the particle's location.

truncating the numerical domain at a finite radius. In [33] both codes enforced zero incoming modes at the outer boundary. Such boundary conditions are typically used for numerical convenience in order to maintain stability, but are clearly unphysical since the tail from the spacetime outside of the numerical domain is ignored. This essentially leads to a non-physical reflection from the outer boundary that will affect the extraction of the self-force as soon as the location of the particle comes into contact with the reflected wave. A simple remedy is of course to push the outer boundary to larger radius, practically delaying the influence of the outer boundary condition. However, this comes at a steep price in computational cost.

The second problem comes from the  $C^0$  nature of the source, leading to the limited  $C^2$  regularity of the scalar field at the particle location. In order to obtain the expected convergence with either high order finite differencing or spectral methods it is required that the fields being evolved are sufficiently smooth (otherwise the error estimates based on Taylor expansions do not hold). With  $C^2$  fields, the extracted self-force only converges to 2nd order using finite differencing methods and between 4th and 5th order using spectral methods.

#### *Boundary conditions for long-term evolutions*

The outer boundary problem has been solved using the approach described in [39]. The main idea is to use hyperboloidal slices that approach future null infinity ( $\mathcal{I}^+$ ) at a finite coordinate radius. Our starting point is the black hole metric  $\tilde{g}$  in Kerr-Schild form modified by a spatial coordinate transformation in order for the black hole horizon to be a coordinate sphere even in the rotating case. This form of the metric

is particularly well suited to our 3D multi-block code where we have a spherical inner excision boundary (inside the black hole horizon) as well as a spherical outer boundary.

To proceed, we introduce a new time coordinate  $\tau$  related to the standard Kerr-Schild time coordinate  $t$  by

$$\tau = t - h(r), \quad (34)$$

where  $h(r)$  is called the height function. In addition we compactify the radial coordinate

$$r = \frac{\rho}{\Omega}, \quad \text{with} \quad \Omega = \Omega(\rho). \quad (35)$$

To remedy the fact that this leads to the metric  $\tilde{g}$  being singular at  $\Omega = 0$  we additionally perform a conformal rescaling to obtain  $g = \Omega^2 \tilde{g}$ . Under such a conformal rescaling the scalar wave equation satisfies the following conformal transformation rule

$$\left(\square - \frac{1}{6}R\right)\phi = \Omega^{-3} \left(\tilde{\square} - \frac{1}{6}\tilde{R}\right)\tilde{\phi}. \quad (36)$$

Here  $\square$  and  $R$  are the wave operator and Ricci scalar associated with the rescaled metric  $g$ , while the quantities with tildes are associated with the physical metric. The scalar fields  $\phi$  and  $\tilde{\phi}$  are related through  $\phi = \tilde{\phi}/\Omega$ . Note that although  $\tilde{R}$  is zero (since it is a vacuum spacetime) the conformally rescaled  $R$  is non-zero.

In regions where the wave equation is homogeneous (i.e. where  $\mathcal{S}_{\text{eff}}$  is zero) we then have to solve

$$\square\phi - \frac{1}{6}R\phi = 0. \quad (37)$$

In regions where  $\mathcal{S}_{\text{eff}}$  is non-zero, we want to keep things simple and use standard spatial slices, i.e. we want to transition from standard spatial slices near the black hole and source to hyperboloidal slices in the exterior. We do this by suitable choices for  $\Omega(\rho)$  and  $H = dh/dr$

$$\Omega(\rho) = \begin{cases} 1 & \text{for } \rho \leq \rho_{\text{int}} \\ 1 - f + (1 - \rho/S)f & \text{for } \rho_{\text{int}} < \rho < \rho_{\text{ext}}, \\ 1 - \rho/S & \text{for } \rho \geq \rho_{\text{ext}} \end{cases}, \quad (38)$$

$$H(\rho) = dh/dr = \begin{cases} 0 & \text{for } \rho \leq \rho_{\text{int}} \\ \left(1 + \frac{4M\Omega}{\rho} + \frac{(8M^2 - C^2)\Omega^2}{\rho^2}\right) f & \text{for } \rho_{\text{int}} < \rho < \rho_{\text{ext}}. \\ 1 + \frac{4M\Omega}{\rho} + \frac{(8M^2 - C^2)\Omega^2}{\rho^2} & \text{for } \rho \geq \rho_{\text{ext}} \end{cases}. \quad (39)$$

Here  $S$  determines the coordinate location of  $\mathcal{S}^+$ ,  $M$  is the mass of the black hole,  $C$  is a free parameter and  $f$  is a function that smoothly transitions from 1 at  $\rho_{\text{int}}$  to 0 at  $\rho_{\text{ext}}$ .

With this choice, the coordinate speed of in- and outgoing characteristics at  $\rho = S$  are

$$c_- = 0, \quad c_+ = S^2/C^2. \quad (40)$$

By choosing  $C = S$  we can fix the outgoing characteristic speed to  $c_+ = 1$  (much larger values would severely limit the size of time steps we could use). Since  $c_- = 0$



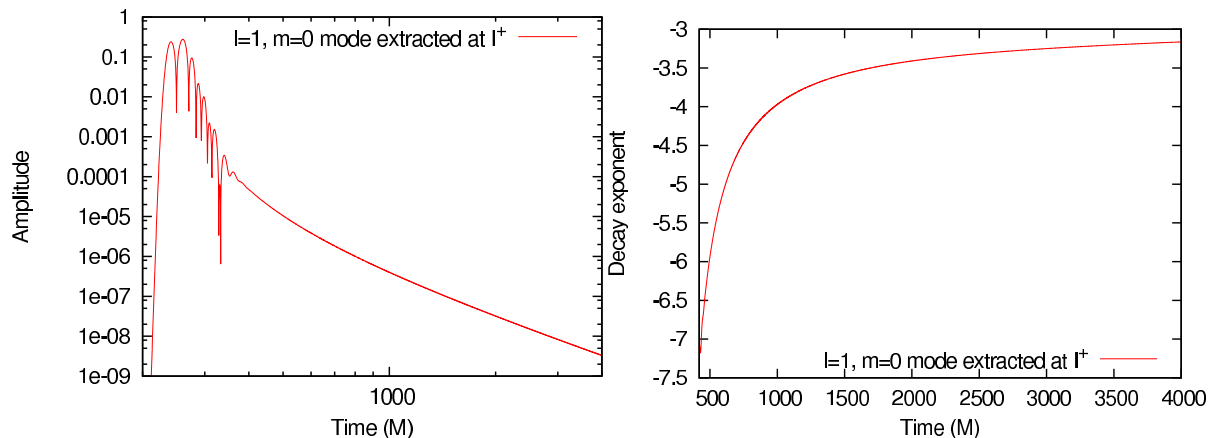


**Figure 3.** (Color online) The left plot shows the  $\ell = 1$ ,  $m = 0$  mode of the scalar field extracted at  $\mathcal{I}^+$  when evolving  $\ell = 1$ ,  $m = 1$  initial data in a Schwarzschild background. The right plot shows the decay exponent of the tail as a function of time.

we have no incoming modes (as expected at  $\mathcal{I}^+$ ) and we then do not have to apply a boundary condition at the outer boundary. This is similar to the situation at the inner boundary, where the presence of a black hole horizon ensures that all modes leave the computational domain. We are therefore in the remarkable situation that we do not have to apply any boundary conditions on either the inner or the outer boundary of the computational domain. It is also worth mentioning that an outgoing wave will reach  $\mathcal{I}^+$  in finite coordinate time.

As a first test of the performance of the new outer boundary condition we evolved  $\ell = 1$ ,  $m = 0$  scalar initial data (with no source) on a Schwarzschild ( $M=1$ ) background with  $S = 100M$  and  $C = 100M$ . The results presented in Figure 3 are based on a simulation with radial resolution  $\Delta\rho = M/15$  and 30 points per patch in the angular directions and using 8th order finite differencing. The inner excision boundary was placed at  $\rho = 1.8M$ , while the transition from spatial slices to hyperboloidal slices occurred between  $\rho = 20M$  and  $\rho = 60M$ . The left plot shows the amplitude of the  $\ell = 1$ ,  $m = 0$  mode extracted at  $\mathcal{I}^+$  ( $\rho = S = 100M$ ) in a log-log plot. The wave first reaches  $\mathcal{I}^+$  at around  $230M$  and we then see quasinormal mode ringdown with a transition into the tail regime. The right plot shows the numerically extracted exponent of the tail decay. At late times it is expected that the tail of a  $\ell = 1$  mode decays as a power law  $\propto t^{-3}$  at  $\mathcal{I}^+$  (see e.g. [40]). Note that this is different from the expectation at timelike infinity  $I^+$  where the tail would decay as a power law with exponent  $-(2\ell + 3) = -5$ . As can be seen from the plot, we are approaching the value  $-3$  for the decay exponent at late times. Note that the total evolution time is  $4000M$ , which is many times more than the crossing time, and there are no visible effects from either the inner or the outer boundary. This is a very strict test, since it only takes minor numerical errors or inconsistencies to significantly affect the tail behavior.

As a second test we repeated the simulation in [33], that is a scalar point charge on a circular orbit of radius  $10M$  in Schwarzschild spacetime. The simulation in [33]

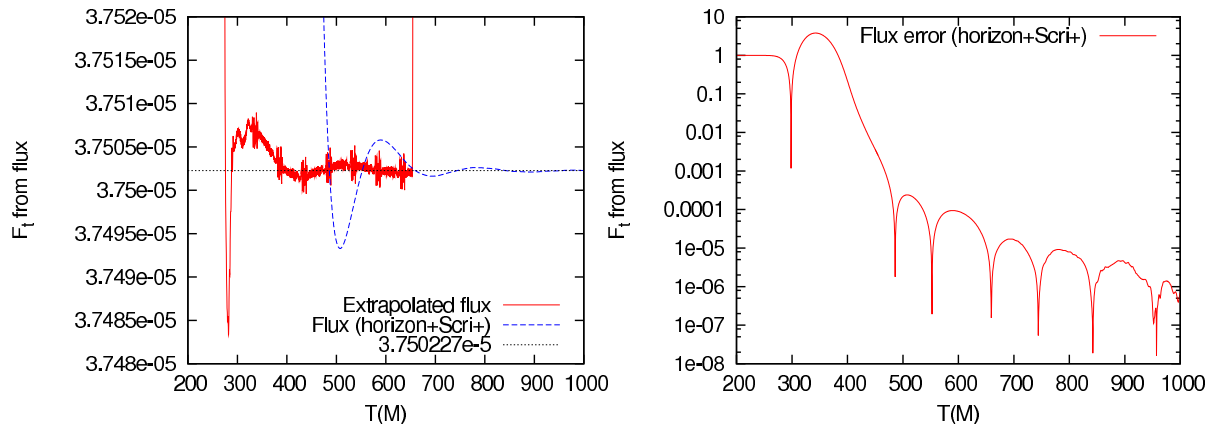


**Figure 4.** (Color online) The left plot shows a comparison of the extraction of the flux done at finite radii and Richardson extrapolated to spatial infinity (red solid line) with the extraction of the flux at  $\mathcal{S}^+$  (blue dashed line). The black dotted line, shows the result from highly accurate results from a frequency domain code. The right plot shows a log plot of the relative error in the extraction of the flux at  $\mathcal{S}^+$ , measured against the frequency domain result.

was performed with the outer boundary located at  $r = 600M$ , while the new simulation was performed with  $\mathcal{S}^+$  located at a coordinate radius of  $\rho = 100M$ . This means that the computational cost of the new simulation was about a factor of 6 smaller than the old one. The angular resolution was kept the same (40 points per patch). In the new run the source was turned on smoothly over one orbit. This was done to avoid an issue with under-resolving the spurious wave generated by turning on the source instantaneously. In the old simulation the coordinate speed of the outgoing characteristics is a monotonically increasing function (approaching 1 as the coordinate radius  $r \rightarrow \infty$ ), while in the new simulation, due to the transition from spatial to hyperboloidal slices, the coordinate speed drops to a minimum of about 0.2 in the transition region and then increases to 1 at  $\rho = S$ . This has the effect that any outgoing wave experiences a compression by about a factor of 5 as it travels through the transition region. Turning on the source slowly ensures that the spurious wave generated initially has long enough wavelength that it is never under-resolved.

The comparison of the best extracted fluxes are shown in the left plot of Figure 4. The fluxes shown are the sum of the fluxes going into the black hole and the outgoing fluxes at infinity converted to the corresponding time component of the self-force. Since, in a time domain calculation, the source is turned on at some point in time, it is expected that it takes some time to reach a helically symmetric state and thus the flux will start out being completely wrong (i.e. zero) and only reach the correct value asymptotically. This can be seen for both the solid (red) and dashed (blue) curves. The solid (red) curve is produced by extracting the flux at several radii (from  $50M$  to  $300M$ ) and then Richardson extrapolated (taking care to time shift accordingly to the light travel time from detector to detector) to spatial infinity. As a result there is some high frequency noise. In addition the curve terminates at  $T = 650M$  when the outermost detector comes

into causal contact with the initial spurious pulse hitting the outer boundary. In order to extend the curve, we would have to redo the simulation with the outer boundary even further out. In contrast, the dashed (blue) curve is very smooth and shows no boundary effects for the duration of the simulation, even with the outer boundary located at  $\rho = 100M$ . This is expected to continue for as long as we would care to extend the simulation time. The right plot in Figure 4 shows the relative error in the flux extraction as a function of time. After about 5 orbits we have gotten rid of so much of the spurious waves that the relative error is as low as 1 part in a million. This is a quite remarkable accuracy considering this is a full 3D simulation.

#### *Over-all accuracy*

As mentioned above, the accuracy in evaluating the self-force at the location of the particle is limited by the  $C^0$  nature of the effective source  $\mathcal{S}_{\text{eff}}$ . The effect of the non-smoothness of the source on the evaluation of the self-force manifests itself as high frequency noise (the frequency being determined by the time it takes the particle to move from a gridpoint to a neighbouring gridpoint) that only converges away at 2nd order regardless of the finite differencing order used (see [33] for more details).

A possible remedy is to modify the finite differencing stencil near the particle location so that the stencil becomes more and more one sided as the particle location is approached in order to always use smooth data to approximate derivatives. However, experiments in 1D have shown that a straightforward implementation of such adjustable finite differencing stencils leads to an unstable numerical scheme, where high frequency noise develops and blows up on a very short timescale. We have not yet finished exploring possible ways of stabilizing such a scheme, but it is certainly possible that such an approach in the general case is doomed to fail. On a positive note, we have been able to find a stable scheme for the case in 1D where the particle is always located exactly at a grid point. We may be able to take advantage of that in our multiblock infrastructure by covering the neighbourhood of the particle with an extra block that is co-moving with the particle. This co-moving block would be completely contained within a non-moving block. The communication between the blocks would be done with interpolation away from the particle location where all fields are smooth. Such an approach would not be possible in the multiblock infrastructure used in [33] but could be implemented in the multiblock infrastructure used in [41] and described in more detail in [42]. It is not yet clear how much infrastructure work such an approach would require.

Finally, an alternative possible remedy is to construct a smoother effective source at the analytical level. This is now possible through the methods of [35], and would result from the inclusion of more terms in the covariant expression for the singular field, as displayed in (27). This would make the coordinate expression for  $\mathcal{S}_{\text{eff}}$  even more complicated than it already is, but this increase in complexity could be mitigated if evaluation of the effective source with numerical derivatives is found adequate. In any case, with a  $C^2$  effective source, the amplitude of the noise would not only be decreased significantly compared to a  $C^0$  source at the lowest resolution currently used,

the convergence would also be 4th order instead of 2nd order, so that small increases in resolution would lead to significantly lower errors.

## 6. Conclusion and future prospects

In this manuscript, we reviewed the foundations underlying the effective source method for self-force calculations. The approach is powerful because it avoids singular sources and fields, thereby obviating the need for any sort of post-processing regularization such as the one performed in the Barack-Ori mode sum method. Moreover, the effective source approach is, in principle, indifferent to the background spacetime, and therefore allows for the evaluation of the self-force on a particle moving on a generic geodesic of an arbitrary curved spacetime.

Not surprisingly, however, the new method comes with its attendant challenges, and we have outlined some of the strategies that may be pursued to overcome them.

Throughout much of the paper, the effective source approach was presented mainly as a technique for evaluating the self-force for a prescribed geodesic orbit in a black hole spacetime. This was done to avoid (as much as possible) having to commit to a specific type of numerical grid (i.e. whether 2+1 or 3+1), as it is important to stress that the use of an effective source is conceptually distinct from this commitment. (Even the use of hyperboloidal slicing, while implemented and tested on a 3+1 grid for this paper, would be beneficial to 2+1 codes as well).

However, one important aspect of the effective source approach is that by avoiding the necessity of any post-processing altogether (e.g. regularization or mode sums), it facilitates the transition from mere self-force computations to the actual self-consistent simulation of the dynamics of both the particle and the field. In the scalar case, all that is necessary is to supplement the field equation for  $\bar{\Phi}^R$  with the equation of motion of the particle:

$$\square\Phi^R = \mathcal{S}_{\text{eff}}(x, x_p, u_p) \quad (41)$$

$$\frac{Du_p^\alpha}{d\tau} = g^{\alpha\beta}(\nabla_\beta\Phi^R)|_{x=x_p}. \quad (42)$$

This set of equations can be simultaneously solved at every timestep on a (3+1) grid. Effective source implementations on (2+1) [29] or (1+1) [31] grids also avoid the need for regularization, but require a post-processing mode sum in order to compute the self-force. In these implementations, one first has to decompose  $\mathcal{S}_{\text{eff}}$  into its spherical- or spheroidal-harmonic components, which are then used as the sources to the corresponding reduced wave equations. Such mode-sum implementations stand to benefit from the inherent symmetries of the Kerr spacetime, and as a result have been demonstrated (in the Schwarzschild case) to lead to more accurate self-force results [32].

A self-consistent evolution of particle-field dynamics has thus far eluded the self-force community, and it would therefore be interesting to see if any surprises arise from it even for the case of the scalar charge. Particularly intriguing are the recently discovered Flanagan-Hinderer resonances [43] that show up only for non-equatorial orbits in Kerr.

With an effective source, it ought to be possible to probe the self-consistent behavior of a scalar charge as it goes through one of these resonances.

A generalization of the effective source approach to the gravitational case is also within reach. All that would be required is the construction of the corresponding effective point mass (in Lorenz gauge), and much of this follows from the methods we have described here. However, the task of then meaningfully involving this effective point mass in a self-consistent scheme will require some thought. The situation in the gravitational case is more complicated than in the scalar case because the former involves an unusual “gauge condition” (strictly, a controlled *violation* of the Lorenz gauge) that must also be satisfied at every time step [10]. It is unclear at the moment how to translate this requirement into a practical framework.

In this paper, we described notable progress on two fronts, mainly (a) the construction of an effective source for a scalar point charge moving along a *generic* geodesic, and (b) the implementation of hyperboloidal slicing to resolve the issue of boundary reflections, which is critical for the long-term evolutions required by the effective source approach. We anticipate that future work shall focus on making much needed refinements to our current effective source, calculating the self-force on scalar charges moving on generic geodesics in Kerr, and finally, studying the self-consistent dynamics of a scalar particle and its field.

## Acknowledgements

We gratefully acknowledge Steve Detweiler and Eric Poisson for valuable discussions. We are also thankful to Sam Dolan, Leor Barack, José Luis Jaramillo, Michael Jasiulek and Erik Schnetter for providing insightful suggestions. Portions of this research were conducted with high performance computational resources provided by the Louisiana Optical Network Initiative (<http://www.loni.org/>). In addition this research was supported in part by the National Science Foundation through TeraGrid resources provided by LSU/NCSA/NICS under grant number TG-MCA02N014. Finally, we would like to express our gratitude to the attendees of the 2010 Capra meeting for many illuminating conversations and to the Perimeter Institute for providing a fruitful environment for the meeting.

## References

- [1] P. Amaro-Seoane, J.R. Gair, M. Freitag, M.C. Miller, I. Mandel, C.J. Cutler, and S. Babak. Intermediate and extreme mass-ratio inspirals – astrophysics, science applications and detection using LISA. *Class. Quantum Grav.*, 24:R113–R169, 2007.
- [2] M. Davis, R. Ruffini, W.H. Press, and R.H. Price. Gravitational radiation from a particle falling radially into Schwarzschild black hole. *Phys. Rev. Lett.*, 27:1466–1469, 1971.
- [3] S.L. Detweiler. Black holes and gravitational waves. I. Circular orbits about a rotating hole. *Astrophys. J.*, 225:687–693, 1978.
- [4] T. Regge and J.A. Wheeler. Stability of a Schwarzschild singularity. *Phys. Rev.*, 108:1063–1069, 1957.

- [5] F.J. Zerilli. Gravitational field of a particle falling in a Schwarzschild geometry analyzed in tensor harmonics. *Phys. Rev. D*, 2:2141–2160, 1970.
- [6] S.A. Teukolsky. Perturbations of a rotating black hole. I. Fundamental equations for gravitational, electromagnetic, and neutrino-field perturbations. *Astrophys. J.*, 185:635–647, 1973.
- [7] Y. Mino, M. Sasaki, and T. Tanaka. Gravitational radiation reaction to a particle motion. *Phys. Rev. D*, 55:3457–3476, 1997.
- [8] T.C. Quinn and R.M. Wald. Axiomatic approach to electromagnetic and gravitational radiation reaction of particles in curved spacetime. *Phys. Rev. D*, 56:3381–3394, 1997.
- [9] T.C. Quinn. Axiomatic approach to radiation reaction of scalar point particles in curved spacetime. *Phys. Rev. D*, 62:064029–1–064029–9, 2000.
- [10] Samuel E. Gralla and Robert M. Wald. A Rigorous Derivation of Gravitational Self-force. *Class. Quant. Grav.*, 25:205009, 2008.
- [11] A. Pound. Self-consistent gravitational self-force. *Phys. Rev. D*, 81:024023–1–024023–45, 2010.
- [12] L. Barack and A. Ori. Mode sum regularization approach for the self-force in black hole spacetime. *Phys. Rev. D*, 61:061502–1–061502–5, 2000.
- [13] L. Barack. Self-force on a scalar particle in spherically symmetric spacetime via mode-sum regularization: Radial trajectories. *Phys. Rev. D*, 62:084027–1–084027–21, 2000.
- [14] L. Barack and L. Burko. Radiation-reaction force on a particle plunging into a black hole. *Phys. Rev. D*, 62:084040–1–084040–5, 2000.
- [15] L. Barack and C.O. Lousto. Computing the gravitational self-force on a compact object plunging into a Schwarzschild black hole. *Phys. Rev. D*, 66:061502–1–061502–5, 2002.
- [16] L.M. Burko. Self-force on a particle in orbit around a black hole. *Phys. Rev. Lett.*, 84:4529–4532, 2000.
- [17] S. Detweiler, E. Messaritaki, and B.F. Whiting. Self-force of a scalar field for circular orbits about a Schwarzschild black hole. *Phys. Rev. D*, 67:104016–1–104016–18, 2003.
- [18] L.M. Diaz-Rivera, E. Messaritaki, B.F. Whiting, and S. Detweiler. Scalar field self-force effects on orbits about a Schwarzschild black hole. *Phys. Rev. D*, 70:124018–1–124018–14, 2004.
- [19] R. Haas and E. Poisson. Mode-sum regularization of the scalar self-force: Formulation in terms of a tetrad decomposition of the singular field. *Phys. Rev. D*, 74:004009–1–004009–29, 2006.
- [20] L. Barack and N. Sago. Gravitational self-force on a particle in circular orbit around a Schwarzschild black hole. *Phys. Rev. D*, 75:064021–1–064021–25, 2007.
- [21] R. Haas. Scalar self-force on eccentric geodesics in Schwarzschild spacetime: a time-domain computation. *Phys. Rev. D*, 75:124011–1–124011–17, 2007.
- [22] N. Warburton and L. Barack. Self-force on a scalar charge in Kerr spacetime: Circular equatorial orbits. *Phys. Rev. D*, 81:084039–1–084039–17, 2010.
- [23] L. Barack and N. Sago. Gravitational self-force on a particle in eccentric orbit around a schwarzschild black hole. *Phys. Rev. D*, 81:084021–1–084021–35, 2010.
- [24] L. Barack and A. Ori. Regularization parameters for the self-force in Schwarzschild spacetime: scalar case. *Phys. Rev. D*, 66:084022–1–084022–15, 2002.
- [25] L. Barack and A. Ori. Regularization parameters for the self-force in Schwarzschild spacetime. II. Gravitational and electromagnetic cases. *Phys. Rev. D*, 67:024029–1–024029–11, 2003.
- [26] L. Barack and A. Ori. Gravitational Self-Force on a Particle Orbiting a Kerr Black Hole. *Phys. Rev. Lett.*, 90:111101–1–111101–4, 2003.
- [27] S. Detweiler and B.F. Whiting. Self-force via a Green’s function decomposition. *Phys. Rev. D*, 67:024025–1–024025–5, 2003.
- [28] P.A.M. Dirac. Classical theory of radiating electrons. *Proc. R. Soc. London, Ser. A*, 167:148, 1938.
- [29] L. Barack and D.A. Golbourn. Scalar-field perturbations from a particle orbiting a black hole using numerical evolution in 2+1 dimensions. *Phys. Rev. D*, 76:044020–1–044020–20, 2007.
- [30] L. Barack, D.A. Golbourn, and N. Sago. m-mode regularization scheme for the self-force in Kerr spacetime. *Phys. Rev. D*, 76:124036–1–124036–14, 2007.



- [31] I. Vega and S. Detweiler. Regularization of fields for self-force problems in curved spacetime: Foundations and a time-domain application. *Phys. Rev. D*, 77:084008–1–084008–14, 2008.
- [32] S.R. Dolan and L. Barack. Self force via m-mode regularization and 2+1D evolution: Foundations and a scalar-field implementation on Schwarzschild. <http://arxiv.org/abs/1010.5255>, 2010.
- [33] I. Vega, P. Diener, W. Tichy, and S. Detweiler. Self-force with (3+1) codes: a primer for numerical relativists. *Phys. Rev. D*, 80:084021–1–084021–22, 2009.
- [34] E. Poisson. The motion of point particles in curved spacetime. *Living Rev. Relativity*, 6, 2004.
- [35] A.C. Ottewill and B. Wardell. A Transport Equation Approach to Calculations of Green functions and HaMiDeW coefficients. <http://arxiv.org/abs/0906.0005>, 2010.
- [36] A.C. Ottewill and B. Wardell. Quasilocal contribution to the scalar self-force: Nongeodesic motion. *Phys. Rev. D*, 79:024031–1–024031–10, 2009.
- [37] K.S. Thorne and J.B. Hartle. Laws of motion and precession for black holes and other bodies. *Phys. Rev. D*, 31:1815–1837, 1985.
- [38] X.-H. Zhang. Multipole expansions of the general-relativistic gravitational field of the external universe. *Phys. Rev. D*, 34:991–1004, 1986.
- [39] Anil Zenginoglu and Manuel Tiglio. Spacelike matching to null infinity. *Phys. Rev.*, D80:024044, 2009.
- [40] Shahar Hod. Mode-coupling in rotating gravitational collapse of a scalar field. *Phys. Rev.*, D61:024033, 2000.
- [41] Denis Pollney, Christian Reisswig, Nils Dorband, Erik Schnetter, and Peter Diener. The Asymptotic Falloff of Local Waveform Measurements in Numerical Relativity. *Phys. Rev.*, D80:121502, 2009.
- [42] Denis Pollney, Christian Reisswig, Erik Schnetter, Nils Dorband, and Peter Diener. High accuracy binary black hole simulations with an extended wave zone. <http://arxiv.org/abs/0910.3803>, 2009.
- [43] E.E. Flanagan and T. Hinderer. Transient resonances in the inspirals of point particles into black holes. <http://arxiv.org/abs/1009.0292>, 2010.